energies

MDPI

Article

The Experimental Investigation of a New Panel Design for Thermoelectric Power Generation to Maximize Output Power Using Solar Radiation

Mohammed A. Qasim [1,2,*], Vladimir I. Velkin [1] and Sergey E. Shcheklein [1]

[1] Nuclear Power Plants and Renewable Energy Sources Department, Ural Federal University, 620002 Yekaterinburg, Russia; v.i.velkin@urfu.ru (V.I.V.); s.e.shcheklein@urfu.ru (S.E.S.)
[2] Department of Projects and Engineering Services, Ministry of Health, Baghdad 10047, Iraq
* Correspondence: mkasim@urfu.ru or mohammed.a.k.qasim@gmail.com

Abstract: It is well established that renewable energy resources for electricity generation are free. In hot areas, solar energy has become one of the major interests of researchers and specialists. This paper aims to experimentally investigate the maximum voltage generation of a thermoelectric generator (TEG) panel. This panel was built from many TEG modules that are connected in series and in parallel. The panel was exposed to high heat due to solar radiation during summer, either directly or through a Fresnel lens. The other side of the TEG panel was cooled using tap water that was passed through aluminum heat exchangers in an active cooling method. It was found that the maximum open-circuit voltage of this TEG panel using a Fresnel lens was 9.35 V. With no lens, it was 11.75 V at 14:00 h local time. The experiments were done during a sunny July period in Iraq.

Keywords: Fresnel lens; heat exchanger; Seebeck; solar radiation; thermoelectric generator

Citation: Qasim, M.A.; Velkin, V.I.; Shcheklein, S.E. The Experimental Investigation of a New Panel Design for Thermoelectric Power Generation to Maximize Output Power Using Solar Radiation. *Energies* **2022**, *15*, 3124. https://doi.org/10.3390/en15093124

Academic Editor: Bertrand Lenoir

Received: 12 March 2022
Accepted: 18 April 2022
Published: 25 April 2022

1. Introduction

Presently, the increasing demand for integrating renewable energy resources and technologies into the infrastructure of utility energy suppliers is deemed a necessity. This is due to increased concerns regarding the issues of global warming and climate change [1]. Despite the huge progress that has been made using renewable energy resources, their efficiency is limited due to the inability to fully convert these energy forms into electricity. There are questions about the competitiveness of alternative energy resources compared to fossil fuel-based systems [2]. One interesting renewable energy technology that converts heat into electricity is thermoelectric generators (TEGs). Thermoelectric generators consist of solid-state devices that utilize the Seebeck effect to convert heat into electrical energy [3–5]. They are normally built from two types of materials: *p*- and *n*-type semiconductors [6]. The temperature difference across a TEG allows for charge carriers to flow, causing electric current generation. The flow of electrical current forms a potential difference across a TEG module, and TEG panels are made by interconnecting many TEG modules [7]. Numerous researchers have employed various types of TEG modules or panels to fabricate innovative designs that utilize thermoelectric generators. Kossyvakis et al. [8] fabricated a hybrid system of PV cells and TEG modules. They employed poly-Si in dye-sensitized solar cells, which were experimentally investigated. Their analysis indicated that TEGs with shorter thermo-elements exhibit improved levels of power output. Moreover, the power output was improved by employing polycrystalline cell dye-sensitized technology. This could be particularly attractive when merging solar cells in PV–TEG hybrids operating under high temperature conditions. Li et al. [9] studied the heat transfer characteristics and the performance of TEGs at various dissipation temperatures at the cold sides of these devices. They fixed the hot side temperature of the TEGs. In their experimental work, they showed that the efficiency of a TEG is increased when the temperature difference

is greater. Teffah and Zhang [10] combined a TEG with a photovoltaic cell as a hybrid system. The hybrid system consisted of a PV cell with a triple junction and a TEG. The TEG absorbed the heat of a PV cell and converted it into electricity. Their design was simulated in MATLAB, and it was verified experimentally. Haiping et al. [11] presented a hybrid system employing a low solar energy concentrating PV and TEG. Their design used a parabolic shaped solar concentrator with a double-glazed PV panel and a heat pipe array of micro-channels. A data acquisition module and a TEG were used to control the system. The TEG was mounted to assist the cold side of the array of heat pipes. Its average thermal efficiency was 45.0%, to which the average efficiency of PV panel, 11.8%, and the daily average TEG electrical efficiency, 0.23%, could be added. Thus, the overall efficiency reaches 57.03%. The experimental work was done during a sunny period in Beijing. Farhangian et al. [12] did an experimental investigation using a solar cavity bounded by a hybrid connection of PV and TEG modules. In the cavity receiver, a decrease in the re-radiation loss of solar energy led to an increase in the unit temperature. In a laboratory setting, the device was exposed to 1000 W/m^2 of simulated solar radiation across its aperture. It was also tested under varying levels of sun irradiation throughout the day. The hybrid system's efficiency peaked at 21.9% during the start of production in the morning when the system was actually exposed to sunshine. K. Karthick et al. [13] presented a TEG design with a heat sink. The heat sink was coupled with a unit called a thermal energy storage (TES) for TEG modular solar reversible generation of power. TEG modules are cooled and heated alternatively through open and closed-circuit conditions. The heat sink, which is packed with a phase change material (PCM), stores thermal energy, allowing for continuous energy from solar power generation at night. The results of this experimental work show that a reversible operation of TEG modules is advantageous for utilizing solar power generation during the day and the night cycles. Wang et al. [14] fabricated a power generator built with four TEGs as half-rings using polymer-based composite materials. Their design was used to recover the waste heat from hot water pipes. In this design, an output voltage of 3.4 mV and an output power of 126 nW were obtained with a temperature difference of 10.5 K. In the simulation, they investigated the effects of thickness and the number of half rings, as well as the effects of the heat sink area and the convective heat transfer coefficient. Riahi et al. [15] studied a hybrid system that concentrated the heat of PV and TEG modules. Their design prototype was experimentally tested. They found that concurrent use of PVs and TEGs gave better results than concentrated heat for a TEG only. Susanto et al. [16] made series and parallel connections of TEG modules that exploited the heat of a rocket stove. The temperature of water in the chamber reached 90 °C. Power generation was done through TEG connections. A test was done by loading a 1–10 kΩ resistor. In the current research, the aim was to develop and to implement a new design of a TEG system and to evaluate the effect of various parameters on its performance. A TEG panel made from many TEG modules was evaluated. The designed system converted solar radiation into electricity. A panel was exposed to solar radiation using either one spot of a Fresnel lens or exposing the panel directly to sunlight. This paper is organized as follows: an introduction is first presented, followed by presentation of a TEG panel design, the proposed experimental methods, results, and a discussion. Economic analysis and cost estimation of system implementation are shown with the conclusions.

2. TEG Panel Design

Normally, a thermoelectric (TEG) module contains up to 100 thermoelectric elements. These elements are based on *p*-type and *n*-type semiconductors [17]. Basically, the working principle of a TEG module is the Seebeck effect. If heat is applied to a TEG module, then the charge carriers off the semiconductor material, which are normally holes in *p*-type and electrons in *n*-type semiconductors, and it will diffuse from an area of higher temperature (T_h) to a lower temperature (T_c) area. Thus, a temperature difference (ΔT) must be available for this change. Diffusion occurs, enabling an electric current, leading to the creation of a voltage potential at the terminals of the TEG module [18]. Owing to these properties, there

are various TEG module configurations and applications [19]. A suitable ΔT enables heat transfer and subsequent electron flow from the *n*-type to the *p*-type semiconductors and the generated voltage is as follows:

$$Voc = \alpha \times \Delta T \tag{1}$$

$$\Delta T = T_h - T_c \tag{2}$$

$$\alpha = (\alpha_p - \alpha_n) \tag{3}$$

where Voc is an open circuit voltage, α is the Seebeck effect coefficient (V/K), while α_p and α_n are the Seebeck coefficients of the *p*-type and the *n*-type TE legs, respectively.

$$\alpha = \Delta v / \Delta T \tag{4}$$

where, Δv , ΔT are the change in voltage and temperature, respectively.

The electrical power of a TEG throughout the external load caused a flow current in the circuit, which can be calculated using power balancing formulas below [20]

$$W = Q_h - Q_c = V.I \tag{5}$$

where, Q_h , Q_c represent the rate of absorbed and dissipated heat at the hot and cold junctions of a TEG module. It can be determined by

$$Q_h = (K_p + k_n)(T_h - T_c) + (\alpha_p - \alpha_n) I T_h - \frac{I^2 R}{2} \tag{6}$$

$$Q_c = (K_p + k_n)(T_h - T_c) + (\alpha_p - \alpha_n) I T_c + \frac{I^2 R}{2} \tag{7}$$

K_p denotes thermal conductivities of the *p*-type, and k_n denotes the thermal conductivities of the *n*-type TEG legs. T_h and T_c are the hot and the cold junction temperatures. While R, I, represent electrical resistance and current, respectively.

Rearranging and simplifying Equations (6) and (7) yields:

$$V = (\alpha_p - \alpha_n)(T_h - T_c) - IR \tag{8}$$

The specifications of a single TEG module are listed in Table 1 [21].

Table 1. Specifications of a single TEG module.

Specification	Value
Material	Ceramic/bismuth telluride
Parametric model	SP1848-27145
Temperature	150 °C
Open-circuit voltage	4.8 V
Color	White
Weight	25 g
Size	(4 × 4 × 0.4) cm (Length × Width × Height)

In this research, the designed TEG panel consisted of 150 TEG modules. The panel had 10 TEG modules connected to form a group in series. Additionally, there were 15 lines connected in parallel, as depicted in Figure 1.

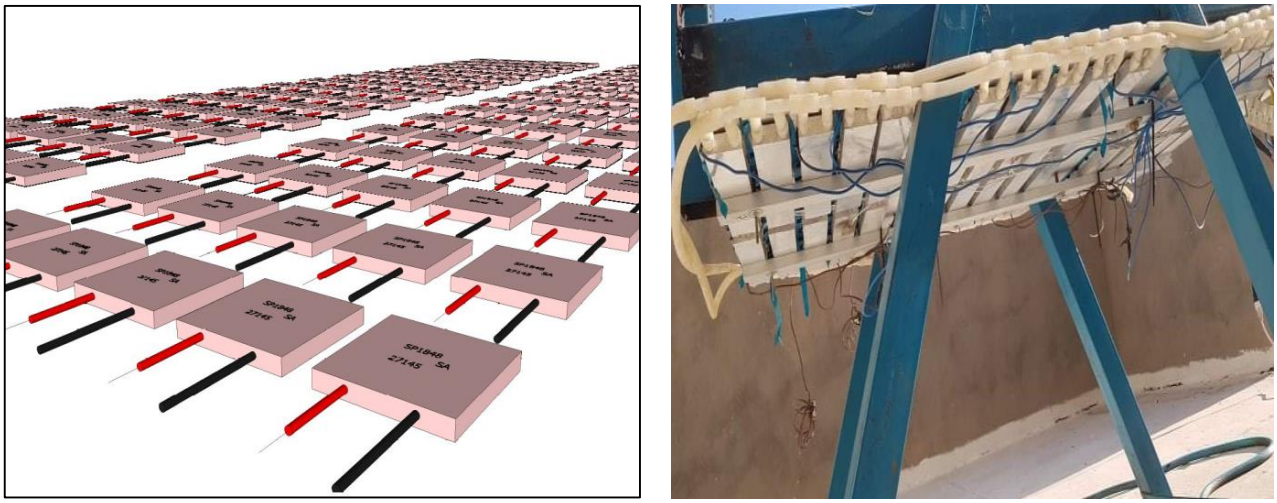

(**a**) (**b**)

Figure 1. TEG modules (**a**) Connected in series and parallel and (**b**) After integration into the system.

3. Experimental Methods

The aim of this research is to maximize the output voltage of a TEG panel. Solar radiation is the heat source while the low temperature sink is normal tap water. Experimental work was done during a hot and sunny July period in Iraq. The TEG panel was placed flat on a table. Its hot surface was covered with a 4 mm thick glass sheet. The distance between the glass cover and the hot surface of the TEG panel was 5 cm. The glass cover served to increase the heat transfer on the hot surface, especially when it was exposed to solar radiation. Additionally, the hot side used a 16 mm thick black aluminum plate mounted directly above the TEG panel to increase heat recovered from solar radiation. On the other side of the TEG panel, 30 heat exchangers were installed to cool the unit with the tap water at a flow velocity of 0.8 m/s. Each heat exchanger was a 40 × 240 × 10 mm "ClYXGS Aluminum Water Cooling Block" [22]. Water cools each heat exchanger to ensure a good temperature distribution on the low temperature side of the TEG panel. Numerous temperature sensors were placed on both sides of the TEG panel. Figure 2 shows a schematic cross-section of the designed TEG panel. The coolant that we employed in this study retained its low temperature, and it did not leak from the system. The installation was done with thermal paste to enable good contact between the TEG and the cooling block. The application of sufficient thermal paste was very important, and it must be used carefully to maximized the contact surface area between the ends of the Peltiers on the panel's back.

To determine the temperature distribution on a test panel, heat sensors (thermocouples) were attached at various places on the panel. These sensors send their measurement signals to an Arduino Mega, connected as shown in Figure 3. The logged measurements were displayed on a serial monitor, and they were saved in a text file. In the current research, two methods were employed to maximize the output voltage of the TEG panel. The first method was application of solar radiation to the TEG panel through a Fresnel lens. The other method applied solar radiation directly with no lens. Both methods are presented as follows. In conducting the experiment, the two TEG panels were operated under the same environmental conditions and at the same solar radiation. The experiment was conducted by comparing two new designs of a TEG panel system. The first design was integrated with a Fresnel lens (L-TEG panel). The second design used no Fresnel lens (NL-TEG panel). In most studies, the researchers used a single TEG module or many modules at various high temperatures. In the current study, we used a TEG module at lower temperatures. The current and the voltage were manually and automatically measured using instruments and a microcontroller, respectively.

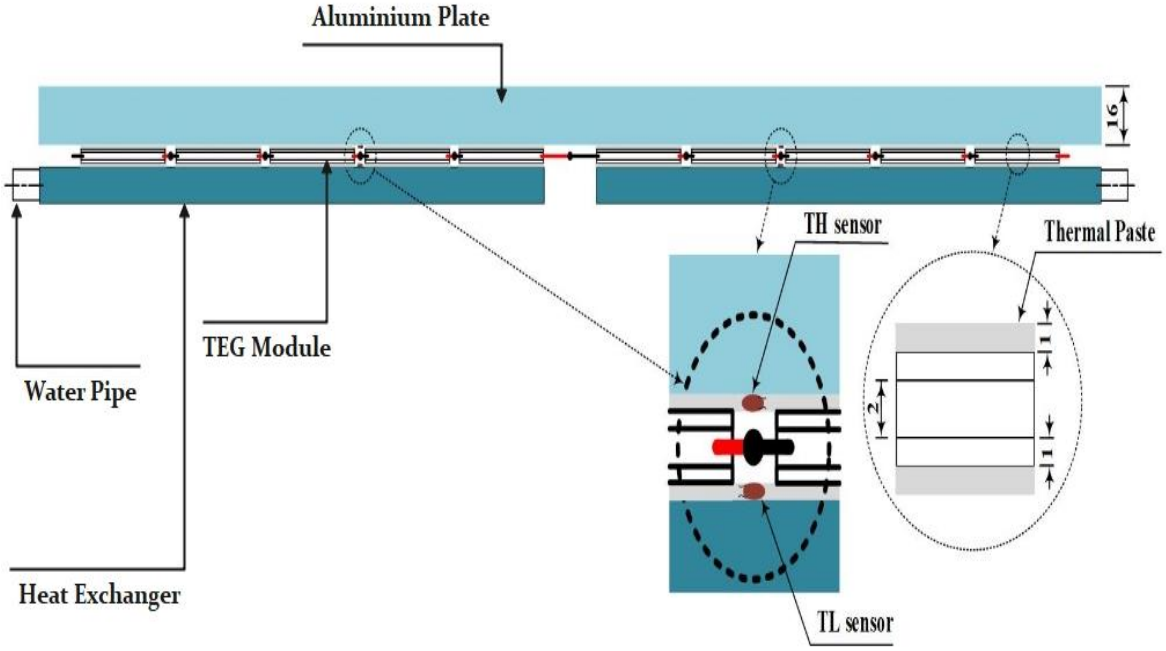

Figure 2. Cross-sectional schematic of the TEG panel.

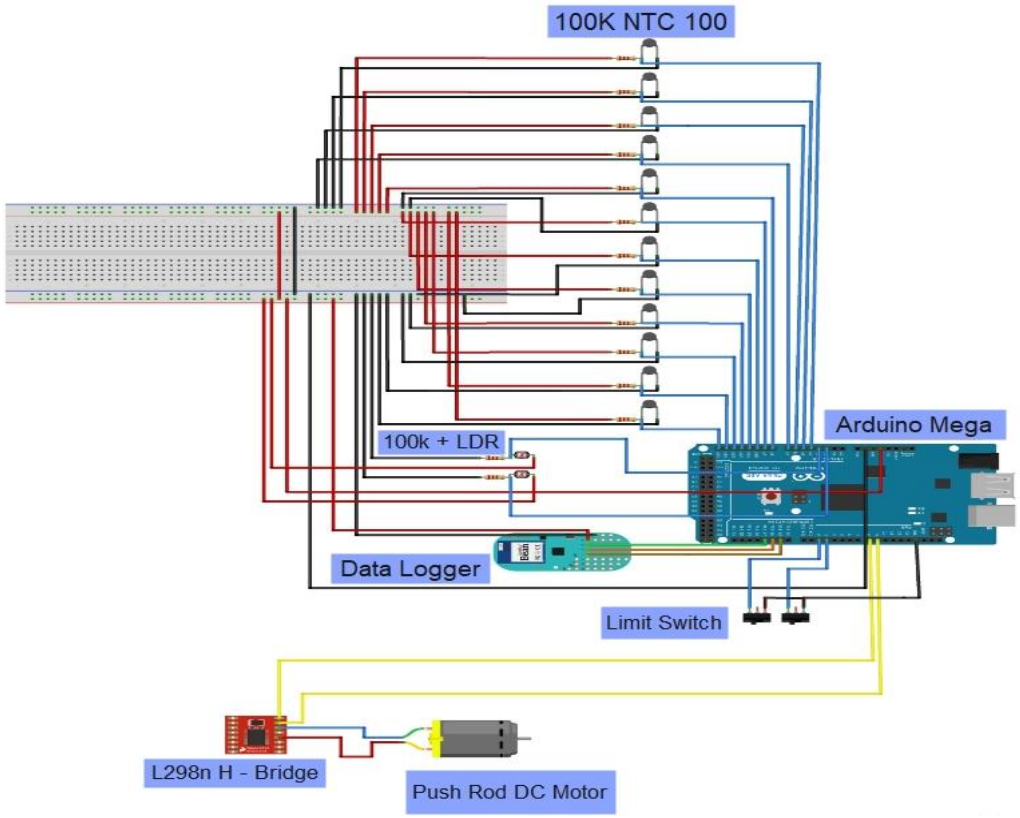

Figure 3. Temperature measurements sent to a data logger via an Arduino Mega.

3.1. Applying Solar Radiation to a TEG Panel through a Fresnel Lens (L-TEG Panel)

In the current study, the proposed approach is unique and simple. A Fresnel lens was used in the L-TEG panel system, while it was not employed in the NL-TEG. A major problem was to provide adequate heat transfer by improving contact with heat and cold sources. This was done using thermal paste in the form of strips placed on both ends of

the Peltiers, which reduced maintenance and replacement costs. There are two kinds of Fresnel lenses. A spot Fresnel lens can focus light onto a single point on a selected place. Conversely, a linear Fresnel lens focuses light onto a line on a selected plane [23,24]. The type of lens used in the current study was a spot Fresnel lens, as depicted in Figure 4. The TEG panel was beneath the lens at a distance equal to its focal length. The Fresnel lens itself was secured by a metal frame. The Fresnel lens dimensions were (1100 × 1100) mm. A linear DC motor was used to adjust the focal length. The tilt angle was controlled via an Arduino Mega microcontroller through a driver circuit, as shown in Figure 3 above.

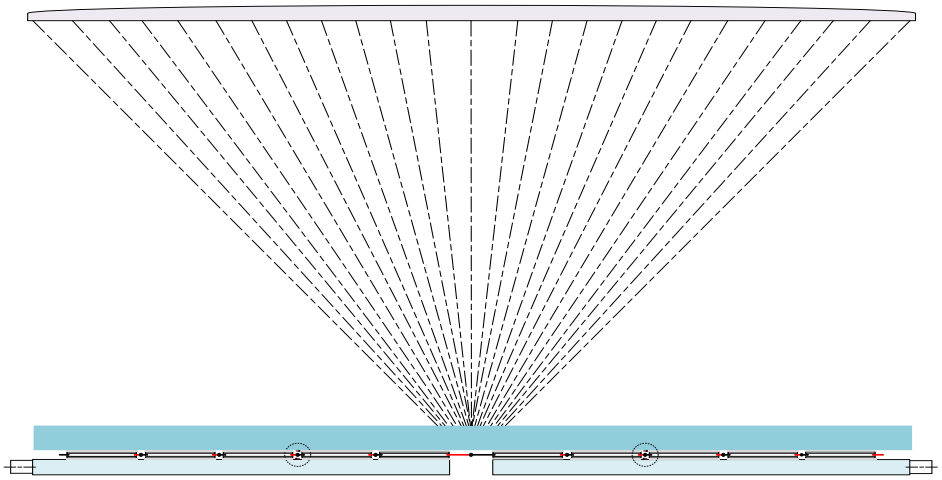

Figure 4. Fresnel lens and the TEG panel (side view).

In our experimental work, a Fresnel lens focused light on a single spot. A glass cover and an aluminum plate ensured an approximately uniform distribution of heat on the hot side of the TEG panel. The entire design was experimentally implemented as shown in Figure 5.

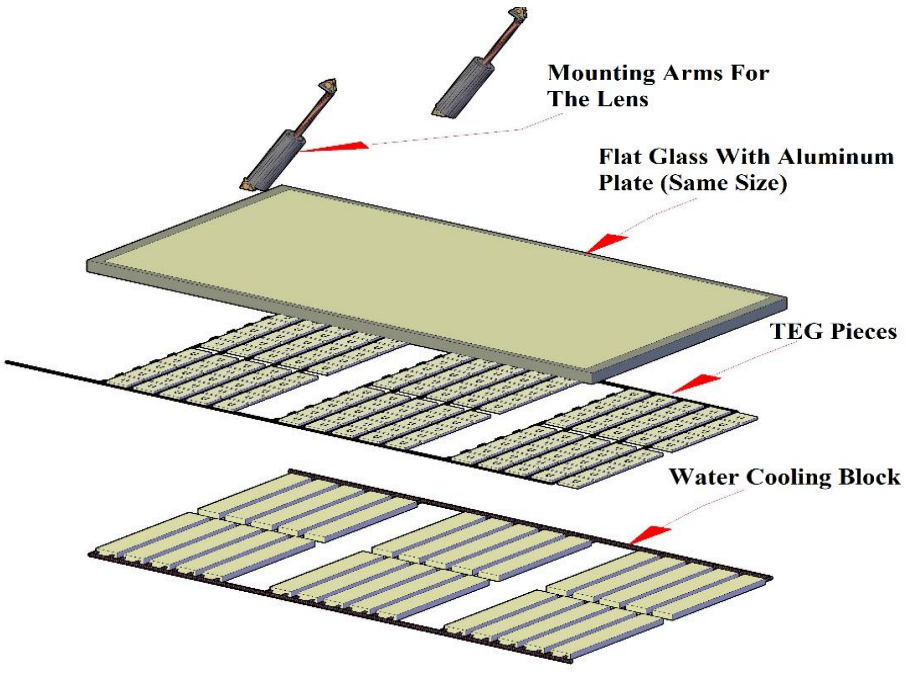

(**a**)

Figure 5. *Cont.*

(**b**)

Figure 5. (**a**) A schematic of the TEG system, (**b**) TEG panel exposed to solar radiation via a Fresnel lens.

3.2. Applying Solar Radiation to a TEG Panel Directly with No Lens (NL-TEG Panel)

In the current experimental work, a TEG panel was exposed to direct solar radiation, as shown in Figure 6. Temperature measurements were logged as described above, i.e., using temperature sensors connected to an Arduino Mega. The TEG panel was oriented for collection of maximal solar radiation during the day. Its panel was aligned using a magnetic compass, compensating for magnetic variation [25]. In the northern hemisphere at latitudes greater than 23.5°, a solar collector should be oriented towards the south. The current study was done at approximately 33° north latitude. Therefore, the TEG panel with no Fresnel lens must face the geographic South Pole to capture maximal solar radiation [26].

(**a**)

Figure 6. *Cont.*

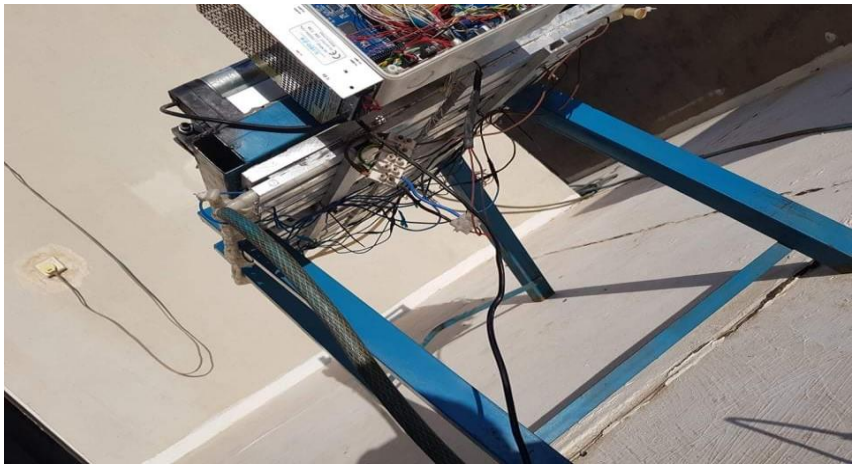

(**b**)

Figure 6. TEG panel exposed to solar radiation with no Fresnel lens, (**a**) Top view, (**b**) Side view.

3.3. Data Reduction

The maximum efficiency of a TEG module is affected by the temperatures on the hot and cold sides as well as the ambient temperature. This is because a module's voltage and its current are affected by its temperature. The maximal efficiency of a TEG module is predicted according to Equation (9) [27–29].

$$\eta_{max} = \frac{T_h - T_C}{T_h} \frac{\sqrt{1+Z\overline{T}}-1}{\sqrt{1+Z\overline{T}}+\frac{T_c}{T_h}} \tag{9}$$

where $\overline{T} = \frac{T_h + T_c}{2}$, T_h and T_c are source and sink temperatures, respectively. $Z\overline{T}$ is called a figure of merit, the thermoelectric figure of merit Z, which is given by Equation (10) below, predicts the performance of any thermoelectric generator [27,30]:

$$Z_{p,n} = \frac{\alpha^2}{\rho\, k'} \tag{10}$$

where ρ denotes electrical resistance and k denotes thermal conductivity. If linked to the average temperature $\overline{T}$ of the thermoelectric module, this figure of merit may become dimensionless for the p-type and the n-type TE legs. It can be represented by the following equations:

$$Z\overline{T}_{p,n} = \frac{\alpha^2\, \overline{T}}{\rho\, k'} \tag{11}$$

$$Z_{p,n} = \frac{\alpha^2\ \sigma}{\lambda} \tag{12}$$

In the above equation α , σ, λ are the Seebeck coefficient, electrical conductivity, and thermal conductivity, respectively. All of these quantities are dependent on the material used for making the TEG, which is Bi_2Te_3 in this study. Here $Z\overline{T}$ appears as constant, however, $Z\overline{T}$ has a temperature dependence through Equation (9). For this reason and due to the dependence of $Z\overline{T}$ on the properties of the manufactured materials, we set the value of $Z\overline{T}$ according to the temperature at which the experiment was done in which $Z\overline{T}$ ranged between (0~1). The value of $Z\overline{T}$ was taken (0.85) as indicated by [31].

4. Analysis of Measurement Errors

This section briefly discusses the influences of measurement errors during the experimental work. These include the rate of error of the measurement devices, as well as those of the sensors and the microcontroller (Arduino). In order to quantify the uncertainty

associated with the instruments used for the measurement, a variety of parameters were measured. Table 2 shows the accuracies of the various instruments, including the digital recorder for ambient temperature measurement, humidity meter, digital clamp meter, TES 132 solar power meter, Handheld Pro HVAC CFM anemometer, and NTC single-end glass seal thermistor temperature sensor. Equation (13) can be used to estimate the standard uncertainty u_n [32,33].

$$u_n = \frac{a_n}{\sqrt{3}} \tag{13}$$

where the accuracy of the instrument, as stated by the manufacturer, is denoted by a_n. The uncertainty of z can be estimated using Equation (14) when z depends on several inputs [33].

$$u(z) = \sqrt{\left(\frac{\delta z}{\delta y_1}\right)^2 u^2(w_1) + \left(\frac{\delta z}{\delta y_2}\right)^2 u^2(w_2) + \ldots\ldots + \left(\frac{\delta z}{\delta y_n}\right)^2 u^2(w_n)} \tag{14}$$

where potential errors are given as Δy_1, Δy_2 , $\ldots\ldots \Delta y_n$. The total percent uncertainty in the TEG system used in the current study was 2.61%. This is acceptable in a system such as the one used in our experiments.

Table 2. Accuracies and uncertainties of various instruments.

Instrument	Range	Accuracy	Uncertainty, %
Digital Temperature Humidity Meter, °C, RH%	−20 °C ∼ 70 °C 0 ∼ 100%RH	±1.0 °C% ±3.0%RH	0.58 1.73
AC/DC Digital Clamp Meter, V	−20 °C ∼ 70 °C	±0.01%	0.01
TES 132 Solar Power Meter, W/m^2	−0 ∼ 2000 W/m^2	±0.7%	0.40
Pro HVAC Anemometer Handheld CFM Meter Wind Speed Meter, m/s	0.001 ∼ 45 m/s	±3%	1.73
NTC single-end glass seal thermistor temperature sensor	−200 ∼ 260	±1%	0.58

5. Results and Discussion

In both experiments, the total time was 240 min. The experiments started at 11:30 h., and it ended at 15.30 h. local time, lasting four hours. The weather, effect of the Fresnel lens, power production, and maximum efficiencies of the two panels are presented and discussed in this section.

5.1. Weather during the Experiments

The weather during the experiments was recorded (see Figure 7). The highest solar radiation, 950 W/m^2, was recorded at 11:30 h Conversely, the lowest solar radiation, 200 W/m^2, was observed at 17:00 h although the data collection period ended at 15:30 h. Over the course of the day, the average solar radiation was 694.59 W/m^2. The highest ambient temperature, 46.8 °C, was recorded at 17:00 h. while the lowest temperature was at around mid-day, 11:30 h., at the start of the experiments. The average temperature during the experiments was 44.91 °C.

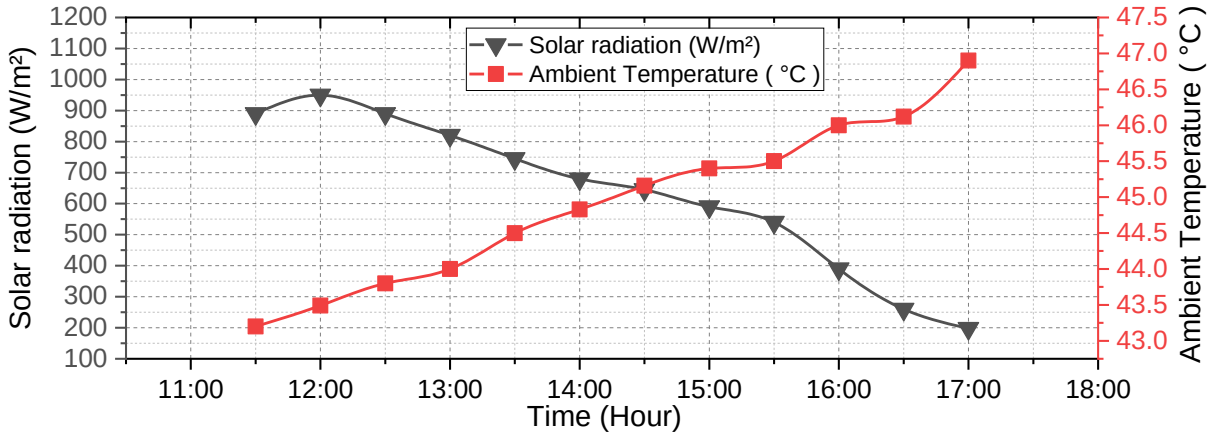

Figure 7. Solar radiation and ambient temperature for the L-TEG and NL-TEG during the day of the experiment.

5.2. Effect of Fresnel Lens at Different ΔT Values on the TEG System

This section discusses the impact of the Fresnel lens on the electrical performance of the two TEG systems. The influence of the devices presented in this research on the thermoelectric system has been investigated, as well as the extent to which they can be employed to save time and effort in the future. As can be seen from Figure 8, the NL-TEG presented the highest ΔT across the TEG modules throughout the experiments. The highest recorded ΔT between the cold and the hot side of NL-TEG panel was at 13:05 h. local time. The ΔT of the NL-TEG showed uniform changes and higher values compared to the L-TEG. The reason for this is that a Fresnel lens focuses solar radiation on a single spot which yields an irregular temperature distribution on the hot side that affects even the lower or the cold side temperature of the TEG panel. In comparison, the NL-TEG panel showed its highest ΔT, 35.62 °C, against 29.18 °C for the L-TEG panel during the same period. The system with no Fresnel lens worked very well, even at quite high temperatures. The mean ΔT for an NL-TEG panel during the experiments was 31.69 °C and 25.80 °C for the L-TEG. This is a 5.89 °C reduction for the NL-TEG, as shown in Figure 9. In both systems, there was an enhanced temperature difference, even though the systems operated under relatively low temperatures. This was attributed to the use of M-shaped cooling blocks, so that the temperature rise on the cold side was reduced compared to previous research [34].

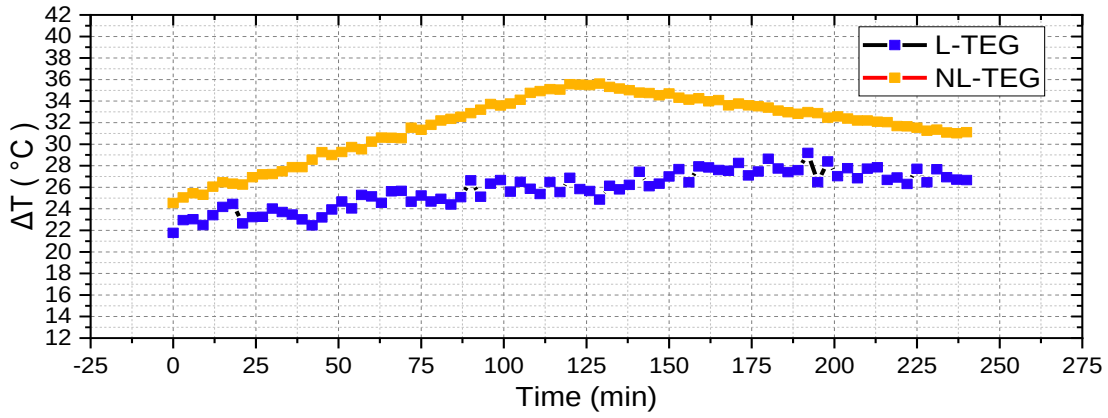

Figure 8. ΔT for each of NL-TEG and L-TEG system.

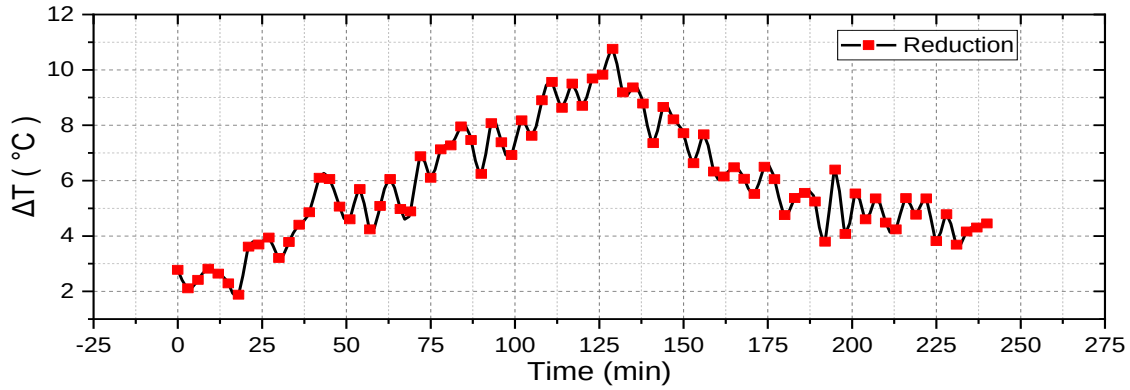

Figure 9. ΔT reduction for each of NL-TEG and L-TEG systems.

5.3. Electrical Performance of the Module

The experimental electric voltages and currents are illustrated in Figure 10. The voltage dropped considerably with decreasing ΔT. During the experiments, the average voltage for the NL-TEG system was 10.33 V, while the L-TEG panel produced 8.74 V. This was a 1.59 V difference and a significant reduction of the L-TEG panel in the voltage. The proposed NL-TEG mechanism showed its effectiveness during the experiments. The voltage using no Fresnel lens was consistently higher than the L-TEG panel. Similarly, the NL-TEG current was slightly higher than the L-TEG. This was expected since the ΔT value was affected when there was no lens. The NL-TEG panel presented an average current of 1.68 A, while the L-TEG panel produced only 1.36 A. The change was insignificant as both panels produced nearly the same current until after mid-day when the ambient temperature increased sharply, affecting the system temperature.

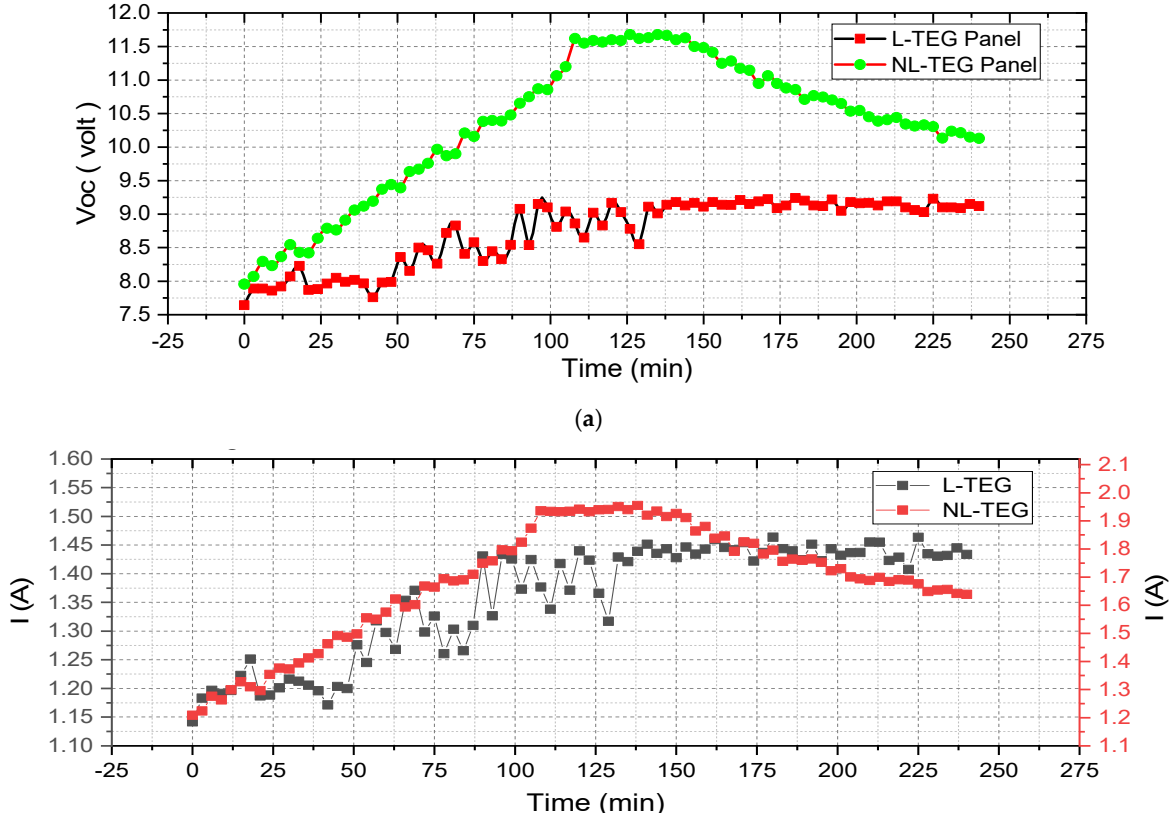

Figure 10. (**a**) Voltage for L-TEG and NL-TEG systems, (**b**) Current for L-TEG and NL-TEG systems.

The power output of both panels is shown in Figure 11. The NL-TEG panel had the highest output power during the experiments. Both panels presented increased power with greater levels of solar radiation, and hence had different temperatures during the experiments. The modules reached their highest temperature differences (ΔT) at exactly 13:00 h However, output power subsequently began to decrease as ΔT decreased due to reduced solar radiation. The NL-TEG presented an average power of 14.37 W versus 9.26 W for the L-TEG panel. Thus, there was a difference of 5.10 W between the panels. This means that a 35.52% improvement in the output power was due to the different temperature profile of the NL-TEG panel.

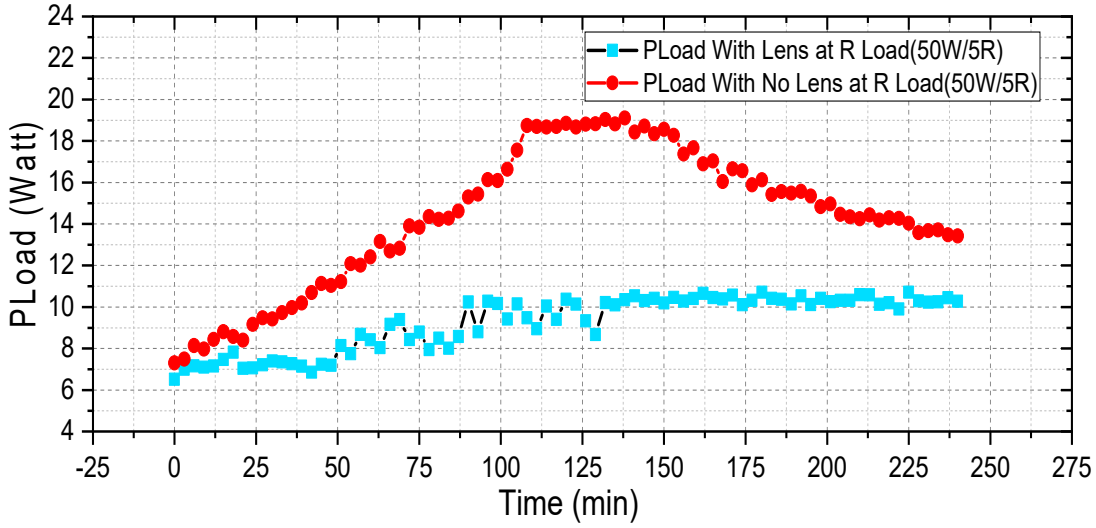

Figure 11. Power for both L-TEG and NL-TEG systems at load of (5 Ω/50 W).

5.4. Maximum Electrical Efficiency for TEG Related to Thermoelectric Materials

The maximum conversion efficiency η_{max} of a TEG module was dependent on the $Z\overline{T}$ of the material used in the fabrication, which was bismuth telluride BI_2 TE_3 here. The differences in the ΔT on the module surface were due to variations in the tap water temperature and solar heat from the sun. The maximum efficiencies of the NL-TEG and L-TEG modules were determined from Equation (9), and Figure 12 presents the results. The calculated average maximum efficiencies realized for the NL-TEG and L-TEG panels were 1.49% and 1.25%, respectively. This represents an improved efficiency of 16.09% in the TEG module, a significant increase since the proposed mechanism does not depend on an active mechanism such as forced convection cooling or heating from outside of the system.

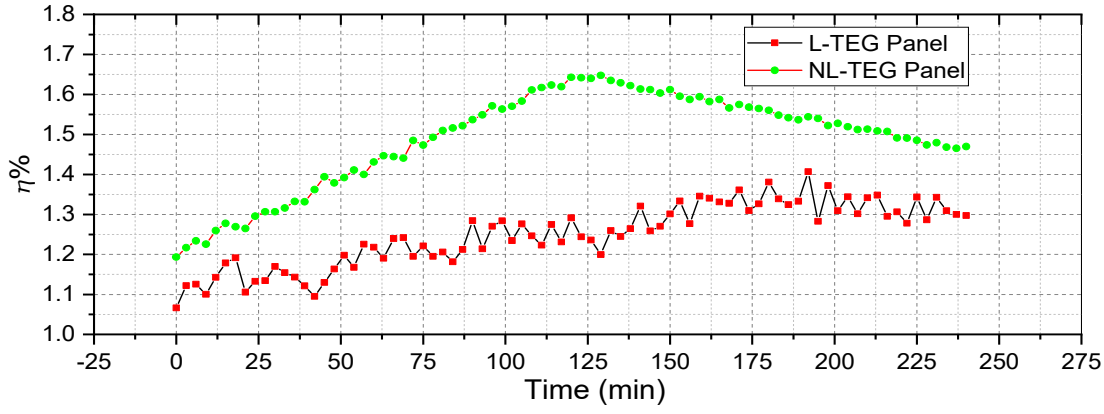

Figure 12. Efficiency for L-TEG and NL-TEG systems.

5.5. Economic Analysis and Cost Estimation of System Implementation

This section presents a cost estimation of such a TEG panel. The estimation is based on the cost of system components. Due to a low generated voltage, the Fresnel lens is excluded from the cost estimation. Table 3 represents the cost of the components of the TEG panel.

Table 3. Component costs of the TEG panel.

Components	Cost US $
TEG module	1.70
Aluminum alloy 6063	15.00
Water cooling Block (Heat Exchanger)	1.10
Glass	2.00
Metal stand	10.00
Flexible plastic water pipes	5.00

The total cost of the entire panel could be reduced if special modules were used to serve as a central heat exchanger with larger TEGs. In comparison with PV cells, TEGs need less maintenance since the former is affected by dust and high temperature, especially during the summer in hot areas like Iraq.

Heat exchangers generally represent much of the thermoelectric generator system costs, which vary from \$1/(W/K) to \$10/(W/K) and higher. Further considerations in economic analysis have been published [35,36] for such systems. The cost of a heat exchanger is expressed in one US dollar per Watt and temperature units (\$/W/K). The lowest thermoelectric cost is found at the maximum power point, but not at the highest power density of the thermoelectric module or the efficiency of the system.

According to the literature [34], the cost of a water-cooling block exchanger is approximately \$13.81/(W/K). Other heat exchangers, such as air-cooled exchangers, have costs of approximately \$15.12/(W/K).

Due to its simplicity and its low initial investment, air-cooled exchangers are most commonly used to improve the efficiency of the hot side of a thermoelectric module, although the actual thermoelectric gain of income is rather modest [35]. Water cooled block exchangers are less costly, more efficient, and help to optimize thermoelectric systems.

6. Conclusions and Future Work

In this paper, a design of a TEG panel is presented as series and parallel connections of 150 TEG elements. Solar radiation is used as a source of heat. The designed unit is exposed to solar radiation either directly or through a Fresnel lens. The conclusions of this work are summarized as follows.

- Throughout a sunny day, even if the solar radiation is decreasing, the ambient temperature is increasing. Normally at 13:00 h., the TEG panel achieves its maximum ΔT at both sides, for both systems (NL-TEG) or (L-TEG). This yields a maximum value of terminal voltage for the TEG panel;
- In an L-TEG system, the ΔT change is not uniform since a Fresnel lens focuses solar radiation over a small area. This creates a nonuniform temperature distribution at the hot side of a TEG panel. Thus, the output power of an NL-TEG is 35.52% higher than for an L-TEG;
- The efficiency of an NL-TEG system is 16.09% higher than an L-TEG system. This efficiency may be increased by more effective cooling.

From the above, an NL-TEG can be used as a cost-effective renewable energy device that can be implemented in hot areas or even integrated with other kinds of renewable energies to maximize the total electricity generated from renewable and the clean sources.

In the future, concave lenses will be used and the entire system will be investigated to ensure a uniform focus and distribution of solar radiation on the TEG panels. Additionally,

the designed TEG panels may be integrated with other renewable energy devices such as PV panels.

It is critical in this unique design of a TEG system at low temperatures differences that consideration be given to using an appropriate heat exchanger to harvest more of the heat rejected from the cold side of the TEG module, as this can affect the thermoelectric output power and efficiency. The results of this design are very valuable for heat recovery applications, exceptionally when employing the sun as a source of thermal energy.

Author Contributions: Conceptualization, M.A.Q. and V.I.V.; methodology, M.A.Q.; software, M.A.Q.; validation, M.A.Q., S.E.S. and V.I.V.; formal analysis, M.A.Q. and V.I.V.; investigation, M.A.Q.; resources, S.E.S. and M.A.Q.; data curation, M.A.Q. and S.E.S.; writing—original draft preparation, M.A.Q.; writing—review and editing, M.A.Q.; visualization, M.A.Q., supervision, V.I.V.; project administration, M.A.Q.; funding acquisition, M.A.Q. All authors have read and agreed to the published version of the manuscript.

Funding: This research received no external funding.

Data Availability Statement: All important data is included in the manuscript.

Acknowledgments: The authors extend their appreciation to Mustafa F. Mohammed and Jeffrey C. Nash, as well as to our university library (URFU), for their support in completing this research.

Conflicts of Interest: The authors declare no conflict of interest.

References

1. Parida, B.; Iniyan, S.; Goic, R. A review of solar photovoltaic technologies. *Renew. Sustain. Energy Rev.* **2011**, *15*, 1625–1636. [CrossRef]
2. Luque, A.; Hegedus, S. *Handbook of Photovoltaic Science and Engineering*, 2nd ed.; Wiley: Chichester, UK, 2011.
3. Riffat, S.B.; Ma, X.L. Thermoelectrics: A review of present and potential applications. *Appl. Therm. Eng.* **2003**, *23*, 913–935. [CrossRef]
4. Tritt, T.M. Thermoelectric Phenomena, Materials, and Applications. *Annu. Rev. Mater. Res.* **2011**, *41*, 433–448. [CrossRef]
5. Bjork, R.; Sarhadi, A.; Pryds, N.; Lindeburg, N.; Viereck, P. A thermoelectric power generating heat exchanger: Part I—Experimental realization. *Energy Convers. Manag.* **2016**, *119*, 473–480. [CrossRef]
6. Emin, D. *Seebeck Effect*; Wiley Online Library: Hoboken, NJ, USA, 2014; pp. 1–14.
7. Qasim, M.A.; Alwan, N.T.; Kumar, S.P.; Velkin, V.I.; Agyekum, E.B. A New Maximum Power Point Tracking Technique for Thermoelectric Generator Modules. *Inventions* **2021**, *6*, 88. [CrossRef]
8. Kossyvakis, D.N.; Voutsinas, G.D.; Hristoforou, E.V. Experimental analysis and performance evaluation of a tandem photovoltaic-thermoelectric hybrid system. *Energy Convers. Manag.* **2016**, *117*, 490–500. [CrossRef]
9. Li, Y.H.; Wu, Z.H.; Xie, H.Q.; Xing, J.J.; Mao, J.H.; Wang, Y.Y.; Li, Z. An experimental investigation of a thermoelectric power generation system with different cold-side heat dissipation. In Proceedings of the 2nd International Conference on New Material and Chemical Industry (NMCI2017), Sanya, China, 18–20 November 2017; IOP Conf. Series; Materials Science and Engineering. 2017; Volume 292, pp. 1–9.
10. Teffah, K.; Zhang, Y. Modeling and experimental research of hybrid PV-thermoelectric system for high concentrated solar energy conversion. *Sol. Energy* **2017**, *157*, 10–19. [CrossRef]
11. Haiping, C.; Jiguang, H.; Heng, Z.; Kai, L.; Haowen, L.; Shuangyin, L. Experimental investigation of a novel low concentrating photovoltaic/thermal-thermoelectric generator hybrid system. *Energy* **2018**, *166*, 83–95. [CrossRef]
12. Marandi, O.F.; Ameri, M.; Adelshahian, B. The experimental investigation of a hybrid photovoltaic-thermoelectric power generator solar cavity-receiver. *Sol. Energy* **2018**, *161*, 38–46. [CrossRef]
13. Karthick, K.; Suresh, S.; Grashin, C.J.; Dhanuskodi, R. Experimental investigation of solar reversible power generation in Thermoelectric Generator (TEG) using thermal energy storage. *Energy Sustain. Dev.* **2019**, *48*, 107–114. [CrossRef]
14. Wang, J.; Liu, S.; Li, L. Experiments and modeling on thermoelectric power generators used for waste heat recovery from hot water pipes. *Energy Procedia* **2019**, *158*, 1052–1058. [CrossRef]
15. Riahi, A.; Ali, A.B.H.; Fadhel, A.; Guizani, A.; Balghouthi, M. Performance investigation of a concentrating photovoltaic thermal hybrid solar system combined with thermoelectric generators. *Energy Convers. Manag.* **2020**, *205*, 1–15. [CrossRef]
16. Susanto, F.; Salim, A.T.A.; Romandoni, N.; Wahyudi, N.; Indarto, B.; Junaedi, Z.M.A.; Basyar, K.A.; Furqan, J.A.; Putra, G.A.B. Application of Thermoelectric Generator TEG Type Parallel Series Electric Circuit Produces Electricity from Heat Rocket Stove. *J. Phys. Conf. Ser.* **2021**, *1845*, 1–8. [CrossRef]
17. Zoui, M.A.; Bentouba, S.; Stocholm, J.G.; Bourouis, M. A Review on Thermoelectric Generators: Progress and Applications. *Energies* **2020**, *13*, 3606. [CrossRef]

18. Electrical4U. Seebeck Effect and Seebeck Coefficient; Last Updated in 31 August 2020 by Electrical4U. Available online: https://www.electrical4u.com/seebeck-effect-and-seebeck-coefficient/ (accessed on 17 April 2022).
19. Qasim, M.A.; Velkin, V.I.; Hassan, A.K. Seebeck Generators and Their Performance in Generating Electricity. *J. Oper. Autom. Power Eng.* **2022**, *10*, 200–205. [CrossRef]
20. Hsu, C.T.; Huang, G.Y.; Chu, H.S.; Yu, B.; Yao, D.J. An effective Seebeck coefficient obtained by experimental results of a thermoelectric generator module. *Appl. Energy* **2011**, *88*, 5173–5179. [CrossRef]
21. Thermoelectric Power Generator TEG Peltier (SP1848-27145). Available online: https://www.amazon.com/SP1848-27145-Thermoelectric-Generator-Temperature-Generation/dp/B07J54H41F (accessed on 17 April 2022).
22. Clyxgs Aluminum Water Cooling Block. Available online: https://www.newegg.com/p/2YM-0045-00255 (accessed on 17 April 2022).
23. Wu, Y.; Eames, P.; Mallick, T.; Sabry, M. Experimental characterisation of a Fresnel lens photovoltaic concentrating system. *Sol. Energy* **2012**, *86*, 430–440. [CrossRef]
24. Rajkrishna, A. Solar Geyser Using Spot Fresnel Lens. *J. Fundam. Renew. Energy Appl.* **2016**, *6*, 1–8. [CrossRef]
25. National Geospatial-Intelligence Agency; Bethesda, M.D. *Handbook of Magnetic Compass Adjustment*; Defense Mapping Agency Hydrographic/Topographic Center: Washington, DC, USA, 2004.
26. Amin, S.; Hanania, J.; Stenhouse, K.; Yyelland, B.; Donev, J. Energy Education—Solar Panel Orientation, 2018. Available online: https://energyeducation.ca/encyclopedia/Solar_panel_orientation (accessed on 17 April 2022).
27. Gaurav, K.; Pandey, S.K. Efficiency calculation of thermoelectric generator by extracting waste heat, for practical applications. *J. Renew. Sustain. Energy* **2017**, *7*, 1–4.
28. Yan, Z.; Song, K.; Xu, L.; Tan, X.; Hu, H.; Sun, P.; Liu, G.; Pan, C.; Jiang, J. Effects of interfacial properties on conversion efficiency of Bi2Te3-based segmented thermoelectric devices. *Appl. Phys. Lett.* **2021**, *119*, 233902. [CrossRef]
29. Qian, D.; Ye, Z.; Pan, L.; Zuo, Z.; Yang, D.; Yan, Y. The Mechanical and Thermoelectric Properties of Bi2Te3-Based Alloy Prepared by Constrained Hot Compression Technique. *Metals* **2021**, *11*, 1060. [CrossRef]
30. Memon, S.; Tahir, K.N. Experimental and Analytical Simulation Analyses on the Electrical Performance of Thermoelectric Generator Modules for Direct and Concentrated Quartz-Halogen Heat Harvesting. *Energies* **2018**, *11*, 3315. [CrossRef]
31. Tritt, T.M.; Subramanian, M.A. Thermoelectric materials, phenomena, and applications: A bird's eye view. *MRS Bull.* **2006**, *31*, 188–198. [CrossRef]
32. Chandrika, V.S.; Karthick, A.; Kumar, N.M.; Kumar, P.M.; Stalin, B.; Ravichandran, M. Experimental analysis of solar concrete collector for residential buildings. *Int. J. Green Energy* **2021**, *18*, 615–623. [CrossRef]
33. Kline, S.J. Describing uncertainty in single sample experiments. *Mech. Eng.* **1953**, *75*, 3–8.
34. Pfeiffelmann, B.; Benim, A.C.; Joos, F. Water-Cooled Thermoelectric Generators for Improved Net Output Power: A Review. *Energies* **2021**, *14*, 8329. [CrossRef]
35. Hendricks, T.J.; Yee, S.; LeBlanc, S. Cost Scaling of a Real-World Exhaust Waste Heat Recovery Thermoelectric Generator: A Deeper Dive. *J. Electron. Mater.* **2016**, *45*, 1751–1761. [CrossRef]
36. Lv, S.; He, W.; Jiang, Q.; Hu, Z.; Liu, X.; Chen, H.; Liu, M. Study of different heat exchange technologies influence on the performance of thermoelectric generators. *Energy Convers. Manag.* **2008**, *156*, 167–177. [CrossRef]